

Quark production in the bottom-up thermalization

Sergio Barrera Cabodevila, Xiaojian Du, Carlos A. Salgado, Bin Wu

Instituto Galego de Física de Altas Enerxías IGFAE, Universidade de Santiago de Compostela, E-15782 Galicia-Spain

Abstract

We investigate the impact of quark production on bottom-up thermalization in heavy-ion collisions. First, we extend the parametric estimates of bottom-up thermalization in pure gluon systems by incorporating quark production in the weak-coupling (high-energy) limit. Our analysis reveals that quark production does not alter the qualitative features of the three-stage thermalization process in this limit. Furthermore, we obtain the scaling behavior of the quark number density over time at each stage. Then, by solving the Boltzmann equation in diffusion approximation (BEDA) for longitudinally boost-invariant systems, we demonstrate how our detailed numerical simulations approach the predicted three-stage thermalization picture as the strong coupling α_s decreases. Finally, we carry out a detailed comparison of our BEDA results with those obtained by solving the QCD effective kinetic theory for intermediate values of α_s , observing remarkably good quantitative agreement between the two approaches.

1. Introduction

One of the most fundamental unresolved theoretical questions in heavy-ion physics is to understand, from QCD first principles, how small droplets of quark-gluon plasma (QGP) emerge in high-energy nucleus-nucleus collisions [1, 2]. While no reliable framework currently exists to describe this process at intermediate or large coupling, a consistent picture is beginning to emerge in the weak-coupling (high-energy) regime within perturbative QCD. According to the concept of parton saturation [3], saturated partons, characterized by the saturation momentum Q_s , are freed from the colliding nuclei, giving rise to a dense partonic system predominantly composed of gluons in the very early stage of the collision [4, 5, 6]. The saturation momentum Q_s at LHC energies is estimated to be about 1-2 GeV, entering the perturbative regime.

In the weak-coupling limit, the subsequent thermalization process of pure gluon systems has been outlined in Ref. [7] through parametric estimates, known as the "bottom-up" thermalization. Quantitative studies have been investigated using weak-coupling techniques, including classical statistical field theory [8, 9] and effective kinetic theory (EKT) [10], as presented in [11, 12, 13, 14]. Classical field approaches are known to break down at later times [15, 16, 17, 18]. It is conventional to switch from classical field simulations to the Boltzmann equation description [7, 15, 19], although how this transition can be understood in perturbation theory remains unclear [20, 21]. To date, EKT has been the only weak-coupling framework used to study quantitatively the entire process of subsequent thermalization/hydrodynamization.

Recently, the Boltzmann equation in diffusion approximation (BEDA) has been solved to explore various aspects of thermalization in spatially homogeneous systems [22, 23]. This set of equations includes both $2 \leftrightarrow 2$ interactions [24, 7, 25, 26, 27] and $1 \leftrightarrow 2$ processes due to the Landau-Pomeranchuk-Migdal (LPM) effects in the deep LPM regime [28, 29]. Using BEDA, parametric estimates for thermalization have been derived for both initially under- and over-populated systems and verified through numerical solutions. Moreover, the results remain qualitatively consistent with those from EKT [30, 31, 13, 12, 14, 32], while benefiting from reduced computational complexity due to the diffusion approximation.

As elaborated in Refs. [31, 22, 23], spatially homogeneous, initially over-populated systems exhibit similarities to the early stage of bottom-up thermalization. This stage is characterized by self-similar solutions, referred to as a nonthermal fixed point in Ref. [8]. The characteristic scaling behavior can be understood via momentum broadening due to multiple elastic scatterings [7], which can be alternatively studied via the adiabatic hydrodynamization approach [33, 34]. On the other hand, initially under-populated systems without expansion also undergo bottom-up ther-

malization in the final stage of thermalization, driven by democratic branching due to the LPM effects [7, 35, 36, 37]. Allowing quark production does not significantly alter the qualitative behavior of initially very dilute or dense systems [23]. However, in non-extreme cases, the system thermalizes in a top-down manner: gluons thermalize first at a higher temperature and gradually cool down to the final equilibrium temperature as quarks are produced [13, 23].

In longitudinally boost-invariant systems, quark production has been recently investigated using EKT [13, 12, 14, 32]. Such theoretical studies are of significance to phenomenological investigations of pre-equilibrium photon [38] and di-lepton production [39, 40, 41, 42], as well as heavy quark thermalization [43] at the early stages of heavy-ion collisions. In this work, we mainly focus on the role played by quark production during the bottom-up thermalization in the weak-coupling limit, providing both parametric estimates and numerical validation. Additionally, we conduct a detailed comparison between BEDA and EKT solutions at intermediate coupling, highlighting their quantitative similarities.

2. The BEDA for longitudinally boost-invariant systems

For a system that is longitudinally boost-invariant and uniform in the transverse plane [44], the QCD Boltzmann equation at midrapidity ($z = 0$) takes the form [24]:

$$\left(\partial_\tau - \frac{p_z}{\tau} \partial_{p_z}\right) f^a = C_{2 \leftrightarrow 2}^a + C_{1 \leftrightarrow 2}^a, \quad (1)$$

where f^a denotes the distribution function of parton a , which varies with time (equal to proper time $\tau \equiv \sqrt{t^2 - z^2}$), momentum magnitude p , and longitudinal velocity $v_z = p_z/p$. Our analysis focuses on the impact of quark production on the entire bottom-up thermalization process, assuming the absence of initial quarks and antiquarks. Consequently, the distribution functions for all N_f massless quark (and antiquark) flavors remain identical, as the Boltzmann equation preserves both $q \leftrightarrow \bar{q}$ symmetry and flavor symmetry. And the effective net quark chemical potentials all vanish. For brevity, we denote the distribution functions for different species as

$$f = f^g, \quad F = f^q = f^{\bar{q}}. \quad (2)$$

As recently detailed in [23], the $2 \leftrightarrow 2$ kernel is simplified using the diffusion approximation [24, 7, 25, 26, 27]:

$$C_{2 \leftrightarrow 2}^a = \frac{1}{4} \hat{q}_a(t) \nabla_p \cdot \left[\nabla_p f^a + \frac{\mathbf{v}}{T^*(t)} f^a (1 + \epsilon_a f^a) \right] + \mathcal{S}_a, \quad (3)$$

where $\epsilon_a = 1$ for bosons and $\epsilon_a = -1$ for fermions and the source terms [27] take the form

$$\mathcal{S}_q = \frac{2\pi\alpha_s^2 C_F^2 \mathcal{L}}{p} \mathcal{I}_c \left[f(1 - F) - F(1 + f) \right], \quad \mathcal{S}_g = -\frac{N_f}{C_F} \mathcal{S}_q. \quad (4)$$

The space-time-dependent quantities in the above equations, which govern the time evolution of the system, are defined as:

1) The jet quenching parameter is defined as $\hat{q}_a \equiv C_a \hat{q}$ [45], where

$$\hat{q} \equiv 8\pi\alpha_s^2 \mathcal{L} \int \frac{d^3 \mathbf{p}}{(2\pi)^3} \left[N_c f(1 + f) + N_f F(1 - F) \right]. \quad (5)$$

Here, C_a takes the values $C_A = N_c$ for gluons and $C_F = (N_c^2 - 1)/(2N_c)$ for quarks/antiquarks. The logarithmic factor is defined as $\mathcal{L} \equiv \ln(\langle p_t^2 \rangle / m_D^2)$. Different choices of the typical transverse momentum broadening $\langle p_t^2 \rangle$ in \mathcal{L} only introduce corrections beyond the leading logarithmic approximation. In this work, it is taken as $\langle p_t^2 \rangle = \hat{q} t_{\text{br}}(\bar{p})$, where the branching time is given by $t_{\text{br}}(p) = \sqrt{p/\hat{q}}/\alpha_s$ [37]. This leads to

$$\mathcal{L} = \ln \left(\frac{\hat{q} t_{\text{br}}(\bar{p})}{m_D^2} \right) = \ln \left(\frac{\sqrt{\hat{q} \bar{p}}}{\alpha_s m_D^2} \right), \quad (6)$$

where the typical momentum \bar{p} is defined as the square root of the average momentum square p^2 per parton, i.e., $\bar{p} = \sqrt{\langle p^2 \rangle}$, and the logarithmic dependence of \hat{q} in the argument of the log on the right-hand side of Eq. (6) is ignored. Under this choice, in a thermalized QGP, we have $\mathcal{L} \sim \ln(1/\alpha_s)$.

2) The effective temperature T_* is defined as

$$T_* \equiv \frac{\hat{q}_A}{\alpha_s N_c \mathcal{L} m_D^2}, \quad (7)$$

where the screening mass squared is given by

$$m_D^2 \equiv 16\pi\alpha_s \int \frac{d^3\mathbf{p}}{(2\pi)^3} \frac{1}{p} (N_c f + N_f F). \quad (8)$$

3) The conversion coefficient, which determines the rate of quark-gluon conversion in $2 \leftrightarrow 2$ scatterings [27], is expressed as

$$\mathcal{I}_c = \int \frac{d^3\mathbf{p}}{(2\pi)^3} \frac{1}{p} (f + F). \quad (9)$$

The $1 \leftrightarrow 2$ kernel includes all the collinear splittings:

$$C_{1 \leftrightarrow 2}^a = \int_0^1 dx \sum_{b,c} \left[\frac{1}{x^3} \frac{\nu_c}{\nu_a} C_{ab}^c(\mathbf{p}/x; \mathbf{p}, \mathbf{p}(1-x)/x) - \frac{1}{2} C_{bc}^a(\mathbf{p}; x\mathbf{p}, (1-x)\mathbf{p}) \right], \quad (10)$$

where x presents the momentum fraction carried by particle b for the process $a \rightarrow bc$, and ν_a is the number of spin times color degrees of freedom for parton a : $\nu_q = 2N_c$ for quarks (antiquarks) and $\nu_g = 2(N_c^2 - 1)$ for gluons. Here, we define

$$C_{bc}^a(\mathbf{p}; x\mathbf{p}, (1-x)\mathbf{p}) \equiv \frac{dI_{a \rightarrow bc}(p)}{dxdt} \mathcal{F}_{bc}^a(\mathbf{p}; x\mathbf{p}, (1-x)\mathbf{p}), \quad (11)$$

and

$$\mathcal{F}_{bc}^a(\mathbf{p}; \mathbf{l}, \mathbf{k}) \equiv f_{\mathbf{p}}^a (1 + \epsilon_b f_{\mathbf{l}}^b) (1 + \epsilon_c f_{\mathbf{k}}^c) - f_{\mathbf{l}}^b f_{\mathbf{k}}^c (1 + \epsilon_a f_{\mathbf{p}}^a) \quad (12)$$

with $\mathbf{l} \equiv x\mathbf{p}$ and $\mathbf{k} \equiv (1-x)\mathbf{p}$. The splitting rates $dI_{a \rightarrow bc}(p)/dxdt$ account for the LPM effects in the deep LPM regime [28, 29]. Their exact expressions in terms of the jet quenching parameter are compiled in Ref. [23]. Here, we highlight the parametric difference between the splittings $a \rightarrow ga$ and $g \rightarrow q\bar{q}$:

$$x \frac{dI_{a \rightarrow ga}(p)}{dxdt} \approx \frac{\alpha_s C_a}{\pi} \sqrt{\frac{\hat{q}_A}{xp}} \quad \text{v.s.} \quad x \frac{dI_{g \rightarrow q\bar{q}}(p)}{dxdt} \approx \frac{\alpha_s}{4\pi} \sqrt{\frac{x\hat{q}_F}{p}} \quad (13)$$

at $x \ll 1$. This leads to a qualitative difference between gluon and quark production via the $1 \rightarrow 2$ processes, as discussed below.

3. Quark production in the bottom-up thermalization

In this section, we study the impact of quark production on the bottom-up thermalization in the weak-coupling limit, based on parametric estimates and numerical simulations in BEDA.

3.1. Parametric estimates

Following Ref. [23], we consider quark production through both the $2 \rightarrow 2$ conversion ($g \rightarrow q/\bar{q}$) and the $1 \rightarrow 2$ splitting ($g \rightarrow q\bar{q}$). Starting with a generic initial gluon distribution $f \sim 1/\alpha_s$ for $p_z \sim p_\perp \sim Q_s$ at $\tau \sim 1/Q_s$, the system evolves through three different stages before transitioning to Bjorken hydrodynamics [44]:

1. *Very early stage: diluting an over-occupied system during* $1 \lesssim Q_s\tau \lesssim \alpha_s^{-3/2}$. During this stage, the system is primarily governed by hard gluons with momentum $\sim Q_s$, similar to pure gluon systems [7]. Its main qualitative features can be deduced from the competition between expansion and multiple $2 \leftrightarrow 2$ scatterings. The number density of hard gluons decreases with time, following $n_{h,g} \sim Q_s^2/(\alpha_s\tau)$. Their longitudinal momentum undergoes broadening by an amount $\sim \sqrt{\hat{q}\tau}$ within a time interval $\sim \tau$. If this broadening is initially negligible compared to their typical longitudinal momentum p_z , then p_z decreases as $1/\tau$ until a balance is reached, yielding [7]:

$$p_z^2 \sim \hat{q}\tau \sim \alpha_s^2 \frac{n_{h,g}^2}{p_z p_\perp^2} \tau \Leftrightarrow p_z \sim Q_s(Q_s\tau)^{-1/3}, \quad f_{h,g} \sim \frac{n_{h,g}}{p_z p_\perp^2} \sim \frac{1}{\alpha_s} \frac{1}{(Q_s\tau)^{2/3}}, \quad \hat{q} \sim \frac{Q_s^3}{(Q_s\tau)^{5/3}}. \quad (14)$$

Here and below, we treat the logarithmic factor \mathcal{L} as an $O(1)$ coefficient and we denote $\hat{q} \sim \hat{q}_A \sim \hat{q}_F$, since the only difference between \hat{q}_A and \hat{q}_F is some parametrically negligible color factor. The Debye mass squared, effective temperature, and conversion coefficient are estimated as:

$$m_D^2 \sim \alpha_s \frac{n_{h,g}}{Q_s} \sim \frac{Q_s}{\tau}, \quad T_* \sim \frac{\hat{q}}{\alpha_s m_D^2} \sim \frac{Q_s}{\alpha_s (Q_s\tau)^{2/3}}, \quad \mathcal{I}_c \sim m_D^2/\alpha_s. \quad (15)$$

The number density of soft gluons with momentum $p_s \sim p_z$, produced via the $1 \rightarrow 2$ splitting, is estimated as follows:

$$n_{s,g} \sim \alpha_s \sqrt{\frac{\hat{q}}{p_s}} n_{h,g} f_{h,g} \tau \sim \frac{Q_s^3}{\alpha_s (Q_s\tau)^{4/3}} \sim T_* p_s^2, \quad f_{s,g} \sim \frac{n_{s,g}}{p_s^3} \sim \frac{1}{\alpha_s (Q_s\tau)^{1/3}} \quad (16)$$

which fills a thermal distribution with temperature given by T_* up to $p \sim p_s$ [22]. Since T_* is initially at its maximum, the soft sector resembles that of an overheated system, similar to what is observed in spatially homogeneous, initially very dense systems [22, 23]. Note that our estimates for soft gluons during this stage and the next, derived solely from the LPM effects, give the same parametric results as those obtained using the BH rate in Ref. [7].

The above estimates remain valid regardless of whether quark production is taken into account. One can estimate the quark number density produced via conversion in Eq. (4) and splitting in Eq. (13):

$$n_q \sim \begin{cases} m_D^4 \tau \sim (Q_s\tau)^{-1} Q_s^3 & \text{for } g \rightarrow q/\bar{q} \\ \alpha_s \sqrt{\hat{q}/Q_s} n_{h,g} \tau \sim (Q_s\tau)^{-5/6} Q_s^3 & \text{for } g \rightarrow q\bar{q} \end{cases}. \quad (17)$$

Here, we have used the fact that $\alpha_s \mathcal{I}_c \sim m_D^2$, as gluons dominate. Comparing the two parametric forms, one can conclude that quark production is primarily driven by the $1 \leftrightarrow 2$ process at this stage, leading to

$$n_q \sim (Q_s\tau)^{-5/6} Q_s^3, \quad (18)$$

which is parametrically smaller than both $n_{h,g}$ and $n_{s,g}$. These quarks mostly carry hard momentum $\sim Q_s$ while the number density of soft quarks with soft momentum $p_s \sim p_z$ is parametrically smaller, scaling as $\sim p_z^3 \sim Q_s^2/\tau$. Consequently, quarks play a negligible role in determining the overall properties of the system at this stage.

Since quarks are absent at initial time ($Q_s\tau \sim 1$), one can directly perform the integration in the collision kernels in Eq. (10) to examine the transition from the initial distribution to the above scaling and obtain

$$n_q \sim \int_{Q_s^{-1}}^\tau d\tau' (\tau' Q_s)^{-11/6} Q_s^4 \sim \frac{Q_s\tau - 1}{(Q_s\tau)^{11/6}} Q_s^3, \quad (19)$$

This result suggests a rapid initial increase in quark number density, reaching a peak shortly after the initial time. Subsequently, it decreases throughout the remainder of this stage.

Accordingly, throughout this stage, corrections to \hat{q} and m_D^2 from soft gluons and quarks do not modify their parametric forms derived from hard gluons. And the pressure anisotropy, dominated by hard gluons as well, scales as

$P_L/\epsilon \sim p_z^2/Q_s^2 \sim (Q_s\tau)^{-2/3}$. Note that during this stage the contribution of soft gluons to the screening mass, given by $m_D^2 \sim \alpha_s n_{s,g}/p_z \sim Q_s/\tau$, remains parametrically comparable to that of hard gluons. This holds until the end of this stage at $Q_s\tau \sim \alpha_s^{-3/2}$ when $f_{h,g} \sim \alpha_s^{-1}(Q_s\tau)^{-2/3} \sim 1$.

2. *Setting up the stage for thermalization: cooling and overcooling of soft sector during $\alpha_s^{-3/2} \lesssim Q_s\tau \lesssim \alpha_s^{-5/2}$.* Primarily driven by expansion, the number density of hard gluons continues to decrease as $n_{h,g} \sim Q_s^2/(\alpha_s\tau)$, since they have not yet suffered significant energy loss. At $Q_s\tau \gtrsim \alpha_s^{-3/2}$, a key change for hard gluons is that $f_{h,g}$ falls below unity. This modifies the scaling of the jet transport parameter to:

$$\hat{q} \sim \alpha_s^2 n_{h,g} \sim \alpha_s Q_s^2/\tau \Rightarrow p_z \sim \sqrt{\hat{q}\tau} \sim \alpha_s^{1/2} Q_s. \quad (20)$$

The soft gluon number density with soft momentum $p_s \sim p_z$ is then given by

$$n_{s,g} \sim \alpha_s \sqrt{\frac{\hat{q}}{p_s}} n_{h,g} \tau \sim \alpha_s^{1/4} (Q_s\tau)^{-1/2} Q_s^3, \quad f_{s,g} \sim \frac{n_{s,g}}{p_s^3} \sim \alpha_s^{-5/4} (Q_s\tau)^{-1/2}. \quad (21)$$

Consequently, the contribution of soft gluons to \hat{q} remains parametrically smaller than that of hard gluons until $Q_s\tau \sim \alpha_s^{-5/2}$ when $n_{s,g} \sim n_{h,g}$. However, soft gluons dominate the contribution to the Debye mass since $n_{h,g}/Q_s \ll n_{s,g}/p_s$, leading to:

$$m_D^2 \sim \alpha_s \frac{n_{s,g}}{p_s} \sim \alpha_s \frac{n_{s,g}}{p_z} \sim \alpha_s^{3/4} (Q_s\tau)^{-1/2} Q_s^2, \quad T_* \sim \frac{\hat{q}}{\alpha_s m_D^2} \sim \alpha_s^{-3/4} (Q_s\tau)^{-1/2} Q_s. \quad (22)$$

These satisfy the relation $n_{s,g} \sim T_*^2 p_z^2$, consistent with a thermal distribution with temperature T_* up to momenta of order p_z .

During this stage, the number of produced quarks remains insufficient to alter the scaling behavior of \hat{q} and m_D^2 . The quark number density is now given by:

$$n_q \sim \begin{cases} m_D^4 \tau \sim \alpha_s^{3/2} Q_s^3 & \text{for } g \rightarrow q/\bar{q} \\ \alpha_s \sqrt{\hat{q}/Q_s} n_{h,g} \tau \sim \alpha_s^{1/2} (Q_s\tau)^{-1/2} Q_s^3 & \text{for } g \rightarrow q\bar{q} \end{cases}. \quad (23)$$

Here, the dominant contributions for $g \rightarrow q\bar{q}$ come from hard gluons. One can also estimate the quark number density from the $g \rightarrow q\bar{q}$ splitting of soft gluons:

$$n_{s,q} \sim \alpha_s \sqrt{\hat{q}/p_s} n_{s,g} \tau \sim \alpha_s \sqrt{\hat{q}/p_z} n_{s,g} \tau \sim \alpha_s^{3/2} Q_s^3. \quad (24)$$

This result is parametrically equivalent to that from the $2 \leftrightarrow 2$ processes and remains negligible compared to the number density of hard quarks until $Q_s\tau \sim \alpha_s^{-2}$ when $n_{s,q} \sim n_q$. Thus, during this stage, the quark number density follows

$$n_q \sim \begin{cases} \alpha_s^{1/2} (Q_s\tau)^{-1/2} Q_s^3 & \text{for } \alpha_s^{-3/2} \lesssim Q_s\tau \lesssim \alpha_s^{-2} \\ \alpha_s^{3/2} Q_s^3 & \text{for } \alpha_s^{-2} \lesssim Q_s\tau \lesssim \alpha_s^{-5/2} \end{cases}. \quad (25)$$

It is parametrically smaller than the gluon number density until $Q_s\tau \sim \alpha_s^{-5/2}$ when $n_q \sim n_{h,g}$. Hence, quarks can be neglected in the parametric estimates of \hat{q} , m_D^2 and other overall properties of the system. Accordingly, the pressure anisotropy scales as $P_L/\epsilon \sim p_z^2/Q_s^2 \sim \alpha_s$.

At $Q_s\tau \sim \alpha_s^{-5/2}$, the number densities of hard gluons, soft gluons, and quarks become comparable. The soft sector forms a thermalized QGP with temperature $T_* \sim \alpha_s Q_s$, where the relaxation time $t_{\text{rel}} \equiv 1/(\alpha_s^2 T_*) \sim \tau$, $p_s \sim T_*$, and $n_q \sim n_{s,g} \sim T_*^3$. Similar to the end of the second thermalization stage in spatially homogeneous, very dilute systems, the soft sector reaches its maximum overcooling in terms of T_* [22, 23].

3. *Thermalization: heating up a QGP bath via mini-jet quenching during $\alpha_s^{-5/2} \lesssim Q_s\tau \lesssim \alpha_s^{-13/5}$.* When $Q_s\tau \gtrsim \alpha_s^{-5/2}$, the contributions from hard gluons to \hat{q} and m_D^2 become parametrically smaller than those from soft gluons and quarks. Additionally, the soft sector can thermalize independently, forming a thermalized QGP with a temperature

T_* , since the relaxation time $t_{\text{rel}} = 1/(\alpha_s^2 T_*)$ becomes smaller than τ . As a result, the system undergoes bottom-up thermalization similar to pure gluon systems, except that the soft thermal bath is now a QGP that is made of quarks, antiquarks and gluons.

More specifically, considering the typical energy loss of each hard parton, $p_{\text{br}} \sim \alpha_s^2 \hat{q} \tau^2$ within a time of order τ [7, 35, 36, 37], the temperature T_* can be estimated from the energy loss of hard partons: $\epsilon_{\text{loss}} \sim T_*^4 \sim p_{\text{br}} n_{h,g}$ with $n_{h,g} \sim Q_s^2/(\alpha_s \tau)$, yielding [7]

$$T_* \sim \alpha_s^3 Q_s^2 \tau \Rightarrow \hat{q} \sim \alpha_s^2 T_*^3 \sim \alpha_s^{11} Q_s^6 \tau^3, \quad m_D^2 \sim \alpha_s T_*^2 \sim \alpha_s^7 Q_s^4 \tau^2, \quad \epsilon_{\text{loss}} \sim T_*^4 \sim \alpha_s^{12} Q_s^8 \tau^4, \quad (26)$$

and the number density of soft partons is given by

$$n_g \sim n_q \sim T_*^3 \sim \alpha_s^9 Q_s^6 \tau^3. \quad (27)$$

As the energy is still predominantly carried by hard gluons and the longitudinal pressure is predominantly given by soft partons, the momentum anisotropy scales as $P_L/\epsilon \sim T_*^4/(Q_s n_{h,g}) \sim \alpha_s^{13} (Q_s \tau)^5$. Thermalization is completed when hard partons are fully quenched, with $\epsilon_{\text{loss}} \sim Q_s n_{h,g}$, which gives $Q_s \tau \sim \alpha_s^{-13/5}$. At this time, the QGP is heated up to $T_* \sim \alpha_s^{2/5} Q_s$ and $P_L/\epsilon \sim 1/3$. All these scalings are the same as those in pure gluon systems [7, 46].

4. *Post-thermalization: Bjorken expansion during $Q_s \tau \gtrsim \alpha_s^{-13/5}$.* After the system thermalizes, it undergoes hydrodynamic expansion with Bjorken flow: $n_g \sim n_q \propto \tau^{-1}$, $T_* \propto \tau^{-1/3}$, $\hat{q} \propto \tau^{-1}$. Starting from their values at $Q_s \tau \sim \alpha_s^{-13/5}$, we have

$$T_* \sim \alpha_s^{-7/15} Q_s (Q_s \tau)^{-1/3}, \quad n_q \sim n_g \sim \alpha_s^{-7/5} Q_s^2 \tau^{-1}, \quad \hat{q} \sim \alpha_s^{3/5} Q_s^2 \tau^{-1}, \quad m_D^2 \sim \alpha_s^{1/15} Q_s^2 (Q_s \tau)^{-2/3}, \quad (28)$$

as one always has the relaxation time $t_{\text{rel}} = 1/(\alpha_s^2 T_*) \ll \tau$.

3.2. Quantitative results

Verifying the scalings of the various quantities estimated above requires a small coupling, which poses a numerical challenge. Since solving BEDA is computationally more efficient, we concentrate on numerical verifications using BEDA in this section and defer a detailed comparison between BEDA and EKT at intermediate coupling to the next section.

To numerically solve the BEDA for longitudinally boost-invariant systems, we extend the GPU algorithm from Ref. [23], originally designed for spatially homogeneous systems, by incorporating the dependence on $v_z = p_z/p$ and longitudinal expansion. The numerical simulations are performed on a lattice in p and v_z , where the grid spacing must be sufficiently small for accuracy but is constrained by finite computing resources and time. For the results presented in this section, we use a logarithmic grid in p with $N_p = 64$ points, ranging from $p_{\text{min}}/Q_s = 0.01$ to $p_{\text{max}}/Q_s = 12$. The v_z grid is symmetric around $v_z = 0$ and it is distributed around it as a power law $v_{z,i} = x_i^{1.3}$, where x_i is the i -th element of a linear grid, and the total number of v_z grid points is set to $N_{v_z} = 64$. With this, the v_z grid is more dense at mid-rapidity, which helps to handle the fact that the distribution functions get very squeezed when the coupling is small. Further details on the implementation of our algorithm will be provided in an upcoming publication [47].

To account for the initial momentum anisotropies, we use the same initial distributions as those used in Ref. [11]:

$$f_0 = \frac{A}{4\pi N_c \alpha_s} \frac{e^{-\frac{2}{3}((p_z \xi)^2 + p_\perp^2)/Q_0^2}}{\sqrt{((p_z \xi)^2 + p_\perp^2)/Q_0^2}}, \quad F = 0, \quad (29)$$

where $Q_0 = 1.8 Q_s$, $A = 10.68$ and the initial momentum anisotropy of the system is parametrized by the variable ξ . In our results the number of active quark flavors is $N_f = 3$.

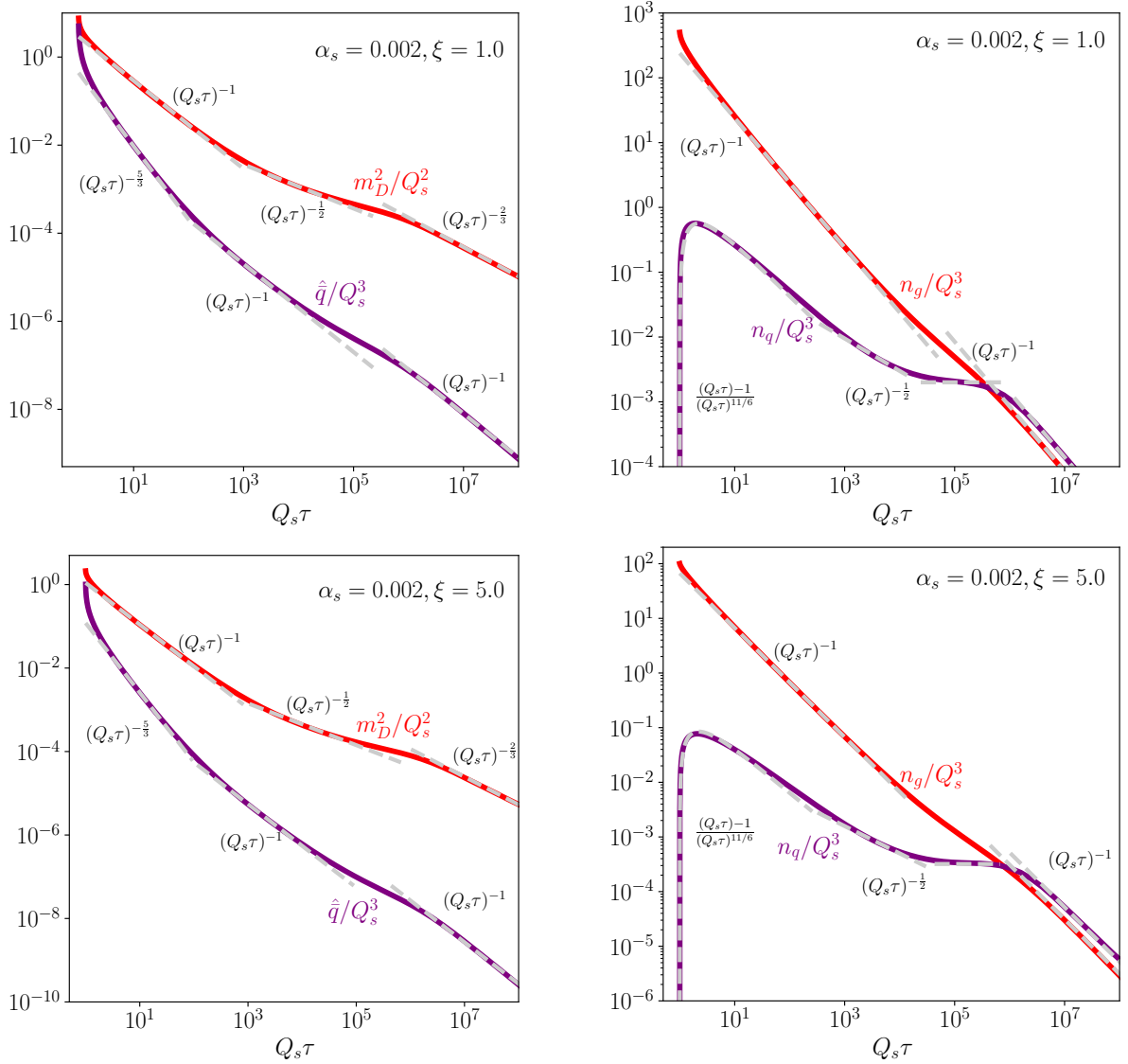


Figure 1: Quark production in the bottom-up thermalization at $\alpha_s = 0.002$. The top and bottom panels display \hat{q} , m_D^2 , n_g and n_q for the initial anisotropies $\xi = 1.0$ and $\xi = 5.0$, respectively. Dashed lines represent the estimated scalings based on parametric estimates, excluding those from the third stage.

Figure 1 shows our simulation results for \hat{q} , m_D^2 , n_g , and n_q at $\alpha_s = 0.002$, compared with the scalings estimated in the previous subsection. We analyze two sets of initial distributions with $\xi = 1$ and $\xi = 5$. As illustrated by the dashed lines, these quantities approach the predicted scalings during the first two stages and at late times in Bjorken hydrodynamics. Importantly, the quark number density remains lower than the gluon density until the final stage of thermalization, consistent with our parametric estimates, confirming that quark production does not interfere with the bottom-up thermalization process. However, for $\alpha_s = 0.002$, the results do not exhibit the scalings in the third stage when \hat{q} and m_D^2 increase with τ , which would require simulations at an even smaller coupling.

In Fig. 2, we further verify the expected scaling in the process of pressure isotropization and hydrodynamization for the same initial conditions as those in Fig. 1. For both cases, P_L/ϵ approaches the expected $\tau^{-2/3}$ scaling [7, 48, 11, 33, 34] at early times. For the isotropic initial distributions shown in the left panel, the expansion drives the momentum anisotropy initially, leading to a scaling $\sim \tau^{-1}$. In late times, they approach the prediction in viscous

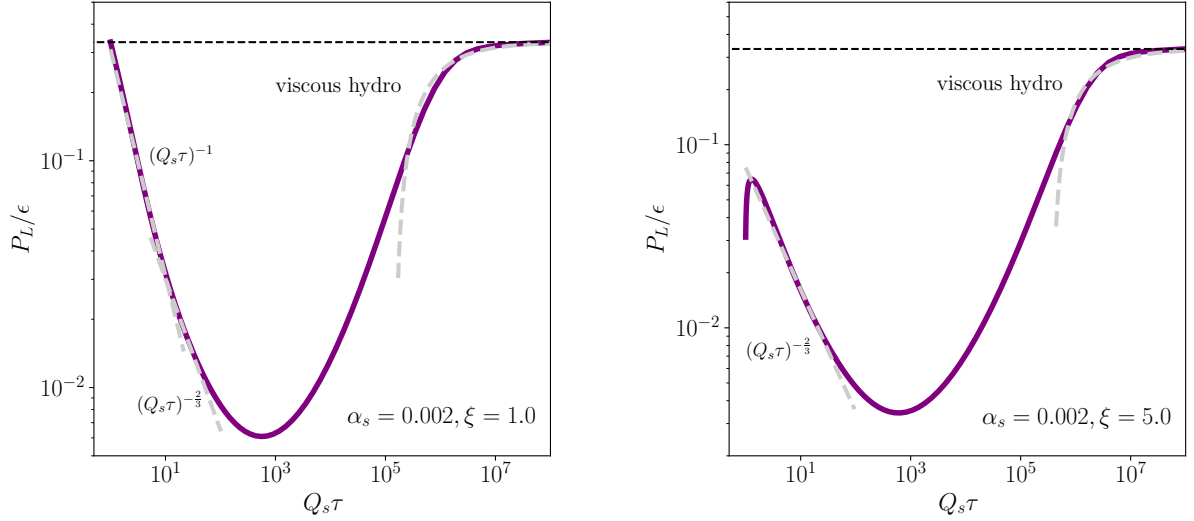


Figure 2: Pressure isotropization and hydrodynamization at $\alpha_s = 0.002$. For both initial distributions with $\xi = 1.0$ (left) and $\xi = 5.0$ (right), our simulations show convergence to the expected scaling at early times as well as hydrodynamization at late times. In both plots, the dashed horizontal line indicates the equilibrium value of $1/3$.

hydrodynamics with

$$\frac{P_L}{\epsilon} = \frac{1}{3} - \frac{16}{9} \frac{\eta}{s} \frac{1}{T_{hydro} \tau}, \quad (30)$$

where the ratio of shear viscosity to entropy density, η/s , is taken as a fitting parameter to our numerical results at late times when $P_L/\epsilon \gtrsim 0.25$, and T_{hydro} is the temperature given by Landau matching:

$$T_{hydro} = \left[\frac{120\epsilon}{\pi^2(4\nu_g + 7N_f\nu_q)} \right]^{\frac{1}{4}} \quad (31)$$

with $\nu_g = 16$ and $\nu_q = 6$.

4. Comparison with EKT at intermediate coupling

To quantitatively compare BEDA and EKT, we carry out a detailed analysis at intermediate coupling using the initial distributions given in Eq. (29), as illustrated in Fig. 3. Here, we set $\xi = 1.0$ and $\alpha_s = 0.265$ ($\lambda \equiv g^2 N_c = 10$), a value relevant to heavy-ion phenomenology at LHC energies. For the BEDA results, we use $N_{v_z} = 64$ and $N_p = 64$ with $p_{min}/Q_s = 0.05$ and $p_{max}/Q_s = 12$. The EKT results shown in these plots are generated using the code implementation from Ref. [14]. For the EKT results, we use a linear grid in v_z with $N_{v_z} = 128$ and the same logarithmic grid in p as BEDA with $N_p = 64$, $p_{min}/Q_s = 0.01$ and $p_{max}/Q_s = 16$.

In Fig. 3, we present the BEDA results using two different choices for the logarithmic factor: $\mathcal{L} = 1.0$, as previously chosen in Refs. [26, 27, 22, 23], and our new choice in Eq. (6). All the quantities shown in this figure are not sensitive to these choices of \mathcal{L} at this coupling. Moreover, T_* , m_D^2 , n_g and P_L^s/ϵ show remarkable agreement with the EKT results over the entire time range, while P_L^q/ϵ , n_q and P_L/ϵ show some quantitative differences. Here, P_L^a denotes the contribution to the longitudinal pressure from parton species a . For a smaller coupling, such as $\lambda = 5$, we have checked that the quantitative agreement between BEDA with \mathcal{L} from Eq. (6) remains comparable to that shown in the figure, but the results with $\mathcal{L} = 1.0$ deteriorate. This confirms that our new choice of \mathcal{L} in Eq. (6) is more consistent than $\mathcal{L} = 1.0$ when comparing to the EKT.

The quantitative difference observed in the bottom plots of Fig. 3 primarily stems from the difference in quark production. Given that at the initial time there are no quarks in the system, the $1 \rightarrow 2$ process is more efficient for producing quarks and antiquarks than the $2 \leftrightarrow 2$ process, qualitatively similar to the weak coupling limit in Sec. 3.

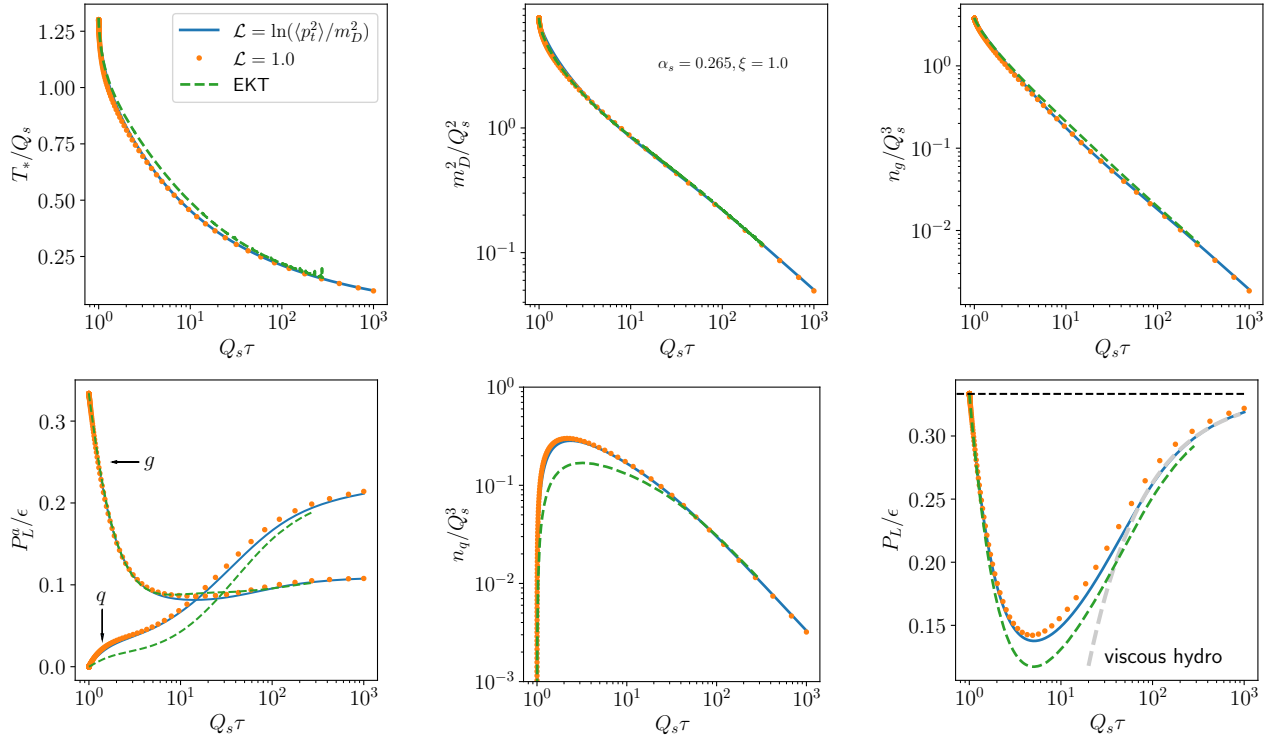


Figure 3: Comparison between BEDA and EKT at $\lambda = 10$ ($\alpha_s = 0.265$). The BEDA results with two different choices of \mathcal{L} are presented for various quantities and compared with the EKT results from Ref. [14]. The top row displays T_* , m_D^2 , and n_g , while the bottom row presents P_L^a/ϵ , n_q and P_L/ϵ . Here, P_L^a denotes the contribution to the longitudinal pressure from parton species a .

For the most relevant momentum range, $p \lesssim Q_s$, we find that the deep LPM splitting rates always have a phase space in x that exceeds the corresponding rates in EKT. As a result, this leads to the overestimation of quark production in the BEDA, as shown in the left two plots of the bottom panel in this figure, as well as the observed difference in P_L/ϵ in the right plot.

Finally, it is intriguing to observe that, even though quark production differs in earlier stages, as the system hydrodynamizes at $Q_s\tau \gtrsim 50$ (see the dashed line in the bottom right panel of Fig. 3), the quark number density in BEDA converges to that in EKT (central bottom panel). This indicates that the system reaches chemical equilibration, as the difference in the gluon number density between BEDA and EKT is remarkably small. That is, the ratio of quark number density to gluon number density converges to the same value in both approaches.

5. Conclusions

In summary, we have extended the parametric estimates for bottom-up thermalization in longitudinally boost-invariant systems [7] by incorporating quark production in the weak-coupling regime. Our analysis demonstrates that quark production does not modify the three-stage thermalization process observed in pure gluon systems, and the system's overall characteristics remain parametrically consistent with those of pure gluons. Quarks and antiquarks become relevant only in the final stage of thermalization, where they form a QGP thermal bath in equilibrium with soft gluons, quenching hard gluons to complete the thermalization process. Additionally, we have investigated the time-dependent scaling behavior of the quark number density across different thermalization stages.

Additionally, we have developed a GPU-based algorithm to numerically solve the BEDA for longitudinally boost-invariant systems. Our detailed simulations using BEDA for $\alpha_s = 0.002$ show that the numerical results generally agree with the predicted scaling behaviors from our parametric estimates, except in the third stage of thermalization, which may only become evident at an even smaller α_s . A comparison between BEDA and EKT for $\alpha_s = 0.265$

demonstrates reasonable agreement, with some noticeable difference in the quark sector, reinforcing BEDA as a valuable and computationally efficient alternative for studying nonequilibrium dynamics in QCD. Future work will focus on extending BEDA simulations to higher dimensions to study thermalization/hydrodynamization in small collision systems.

Acknowledgements

This work is supported by the European Research Council project ERC-2018-ADG-835105 YoctoLHC; by María de Maeztu grant CEX2023-001318-M and by project PID2023-152762NB-I00 both funded by MCIN/AEI/10.13039/501100011033; from the Xunta de Galicia (CIGUS Network of Research Centres) and the European Union. B.W. acknowledges the support of the Ramón y Cajal program with the Grant No. RYC2021-032271-I and the support of Xunta de Galicia under the ED431F 2023/10 project. S.B.C. acknowledges the support of the Axudas de apoio á etapa predoutoral program (Ref. ED481A 2022/279).

References

- [1] S. Schlichting and D. Teaney, *The First fm/c of Heavy-Ion Collisions*, *Ann. Rev. Nucl. Part. Sci.* **69** (2019) 447 [1908.02113].
- [2] J. Berges, M.P. Heller, A. Mazeliauskas and R. Venugopalan, *QCD thermalization: Ab initio approaches and interdisciplinary connections*, *Rev. Mod. Phys.* **93** (2021) 035003 [2005.12299].
- [3] A.H. Mueller, *Parton saturation: An Overview*, in *Cargese Summer School on QCD Perspectives on Hot and Dense Matter*, pp. 45–72, 11, 2001 [hep-ph/0111244].
- [4] J. Jalilian-Marian, A. Kovner, L.D. McLerran and H. Weigert, *The Intrinsic glue distribution at very small x*, *Phys. Rev. D* **55** (1997) 5414 [hep-ph/9606337].
- [5] Y.V. Kovchegov and A.H. Mueller, *Gluon production in current nucleus and nucleon - nucleus collisions in a quasiclassical approximation*, *Nucl. Phys. B* **529** (1998) 451 [hep-ph/9802440].
- [6] A.H. Mueller, *Toward equilibration in the early stages after a high-energy heavy ion collision*, *Nucl. Phys. B* **572** (2000) 227 [hep-ph/9906322].
- [7] R. Baier, A.H. Mueller, D. Schiff and D.T. Son, *'Bottom up' thermalization in heavy ion collisions*, *Phys. Lett. B* **502** (2001) 51 [hep-ph/0009237].
- [8] J. Berges, K. Boguslavski, S. Schlichting and R. Venugopalan, *Turbulent thermalization process in heavy-ion collisions at ultrarelativistic energies*, *Phys. Rev. D* **89** (2014) 074011 [1303.5650].
- [9] T. Epelbaum and F. Gelis, *Pressure isotropization in high energy heavy ion collisions*, *Phys. Rev. Lett.* **111** (2013) 232301 [1307.2214].
- [10] P.B. Arnold, G.D. Moore and L.G. Yaffe, *Effective kinetic theory for high temperature gauge theories*, *JHEP* **01** (2003) 030 [hep-ph/0209353].
- [11] A. Kurkela and Y. Zhu, *Isotropization and hydrodynamization in weakly coupled heavy-ion collisions*, *Phys. Rev. Lett.* **115** (2015) 182301 [1506.06647].
- [12] A. Kurkela and A. Mazeliauskas, *Chemical Equilibration in Hadronic Collisions*, *Phys. Rev. Lett.* **122** (2019) 142301 [1811.03040].
- [13] A. Kurkela and A. Mazeliauskas, *Chemical equilibration in weakly coupled QCD*, *Phys. Rev. D* **99** (2019) 054018 [1811.03068].
- [14] X. Du and S. Schlichting, *Equilibration of weakly coupled QCD plasmas*, *Phys. Rev. D* **104** (2021) 054011 [2012.09079].
- [15] A.H. Mueller and D.T. Son, *On the Equivalence between the Boltzmann equation and classical field theory at large occupation numbers*, *Phys. Lett. B* **582** (2004) 279 [hep-ph/0212198].
- [16] J. Berges, K. Boguslavski, S. Schlichting and R. Venugopalan, *Basin of attraction for turbulent thermalization and the range of validity of classical-statistical simulations*, *JHEP* **05** (2014) 054 [1312.5216].
- [17] T. Epelbaum, F. Gelis and B. Wu, *Nonrenormalizability of the classical statistical approximation*, *Phys. Rev. D* **90** (2014) 065029 [1402.0115].
- [18] T. Epelbaum, F. Gelis, N. Tanji and B. Wu, *Properties of the Boltzmann equation in the classical approximation*, *Phys. Rev. D* **90** (2014) 125032 [1409.0701].
- [19] A. Kurkela, A. Mazeliauskas, J.-F. Paquet, S. Schlichting and D. Teaney, *Effective kinetic description of event-by-event pre-equilibrium dynamics in high-energy heavy-ion collisions*, *Phys. Rev. C* **99** (2019) 034910 [1805.00961].
- [20] B. Wu and Y.V. Kovchegov, *Time-dependent observables in heavy ion collisions. Part I. Setting up the formalism*, *JHEP* **03** (2018) 158 [1709.02866].
- [21] Y.V. Kovchegov and B. Wu, *Time-dependent observables in heavy ion collisions. Part II. In search of pressure isotropization in the φ^4 theory*, *JHEP* **03** (2018) 157 [1709.02868].
- [22] S. Barrera Cabodevila, C.A. Salgado and B. Wu, *Thermalization of gluons in spatially homogeneous systems*, *Phys. Lett. B* **834** (2022) 137491 [2206.12376].
- [23] S.B. Cabodevila, C.A. Salgado and B. Wu, *Quark production and thermalization of the quark-gluon plasma*, *JHEP* **06** (2024) 145 [2311.07450].
- [24] A.H. Mueller, *The Boltzmann equation for gluons at early times after a heavy ion collision*, *Phys. Lett. B* **475** (2000) 220 [hep-ph/9909388].
- [25] J. Hong and D. Teaney, *Spectral densities for hot QCD plasmas in a leading log approximation*, *Phys. Rev. C* **82** (2010) 044908 [1003.0699].

- [26] J.-P. Blaizot, J. Liao and L. McLerran, *Gluon Transport Equation in the Small Angle Approximation and the Onset of Bose-Einstein Condensation*, *Nucl. Phys. A* **920** (2013) 58 [1305.2119].
- [27] J.-P. Blaizot, B. Wu and L. Yan, *Quark production, Bose-Einstein condensates and thermalization of the quark-gluon plasma*, *Nucl. Phys. A* **930** (2014) 139 [1402.5049].
- [28] R. Baier, Y.L. Dokshitzer, A.H. Mueller and D. Schiff, *Medium induced radiative energy loss: Equivalence between the BDMPS and Zakharov formalisms*, *Nucl. Phys. B* **531** (1998) 403 [hep-ph/9804212].
- [29] P.B. Arnold and C. Dogan, *QCD Splitting/Joining Functions at Finite Temperature in the Deep LPM Regime*, *Phys. Rev. D* **78** (2008) 065008 [0804.3359].
- [30] M.C. Abraao York, A. Kurkela, E. Lu and G.D. Moore, *UV cascade in classical Yang-Mills theory via kinetic theory*, *Phys. Rev. D* **89** (2014) 074036 [1401.3751].
- [31] A. Kurkela and E. Lu, *Approach to Equilibrium in Weakly Coupled Non-Abelian Plasmas*, *Phys. Rev. Lett.* **113** (2014) 182301 [1405.6318].
- [32] X. Du and S. Schlichting, *Equilibration of the Quark-Gluon Plasma at Finite Net-Baryon Density in QCD Kinetic Theory*, *Phys. Rev. Lett.* **127** (2021) 122301 [2012.09068].
- [33] J. Brewer, L. Yan and Y. Yin, *Adiabatic hydrodynamization in rapidly-expanding quark-gluon plasma*, *Phys. Lett. B* **816** (2021) 136189 [1910.00021].
- [34] K. Rajagopal, B. Scheihing-Hitschfeld and R. Steinhorst, *Adiabatic Hydrodynamization and the Emergence of Attractors: a Unified Description of Hydrodynamization in Kinetic Theory*, **2405.17545**.
- [35] R. Baier, Y.L. Dokshitzer, A.H. Mueller and D. Schiff, *Quenching of hadron spectra in media*, *JHEP* **09** (2001) 033 [hep-ph/0106347].
- [36] J.-P. Blaizot, E. Iancu and Y. Mehtar-Tani, *Medium-induced QCD cascade: democratic branching and wave turbulence*, *Phys. Rev. Lett.* **111** (2013) 052001 [1301.6102].
- [37] E. Iancu and B. Wu, *Thermalization of mini-jets in a quark-gluon plasma*, *JHEP* **10** (2015) 155 [1506.07871].
- [38] O. Garcia-Montero, A. Mazeliauskas, P. Plaschke and S. Schlichting, *Pre-equilibrium photons from the early stages of heavy-ion collisions*, *JHEP* **03** (2024) 053 [2308.09747].
- [39] M. Coquet, X. Du, J.-Y. Ollitrault, S. Schlichting and M. Winn, *Intermediate mass dileptons as pre-equilibrium probes in heavy ion collisions*, *Phys. Lett. B* **821** (2021) 136626 [2104.07622].
- [40] M. Coquet, X. Du, J.-Y. Ollitrault, S. Schlichting and M. Winn, *Transverse mass scaling of dilepton radiation off a quark-gluon plasma*, *Nucl. Phys. A* **1030** (2023) 122579 [2112.13876].
- [41] M. Coquet, M. Winn, X. Du, J.-Y. Ollitrault and S. Schlichting, *Dilepton Polarization as a Signature of Plasma Anisotropy*, *Phys. Rev. Lett.* **132** (2024) 232301 [2309.00555].
- [42] O. Garcia-Montero, P. Plaschke and S. Schlichting, *Scaling of pre-equilibrium dilepton production in QCD kinetic theory*, *Phys. Rev. D* **111** (2025) 034036 [2403.04846].
- [43] X. Du, *Heavy quark drag and diffusion coefficients in the pre-hydrodynamic QCD plasma*, **2306.02530**.
- [44] J.D. Bjorken, *Highly Relativistic Nucleus-Nucleus Collisions: The Central Rapidity Region*, *Phys. Rev. D* **27** (1983) 140.
- [45] R. Baier, Y.L. Dokshitzer, A.H. Mueller, S. Peigne and D. Schiff, *Radiative energy loss and $p(T)$ broadening of high-energy partons in nuclei*, *Nucl. Phys. B* **484** (1997) 265 [hep-ph/9608322].
- [46] B. Wu, *Early Time Dynamics and Bulk*, *PoS HardProbes2020* (2021) 010 [2009.04974].
- [47] S.B. Cabodevila, X. Du, C.A. Salgado and B. Wu, *work in progress*, .
- [48] S. Schlichting, *Turbulent thermalization of weakly coupled non-abelian plasmas*, *Phys. Rev. D* **86** (2012) 065008 [1207.1450].